Nucleon axial charge from quenched lattice QCD with domain wall fermions

S. Sasaki,[1] K. Orginos,[2] S. Ohta,[3,2] and T. Blum[2]

(RIKEN-BNL-Columbia-KEK Collaboration)

[1]*Department of Physics, University of Tokyo, Tokyo 113-0033, Japan*

[2]*RIKEN BNL Research Center, Brookhaven National Laboratory, Upton, New York 11973, USA*

[3]*Institute of Particle and Nuclear Studies, KEK, Ibaraki 305-0801, Japan*

(Received 9 June 2003; published 30 September 2003)

We present a quenched lattice calculation of the nucleon isovector vector and axial-vector charges g_V and g_A. The chiral symmetry of domain wall fermions makes the calculation of the nucleon axial charge particularly easy since the Ward-Takahashi identity requires the vector and axial-vector currents to have the same renormalization, up to lattice spacing errors of order $O(a^2)$. The doubly blocked Wilson 2 (DBW2) gauge action provides enhancement of the good chiral symmetry properties of domain wall fermions at larger lattice spacing than the conventional Wilson gauge action. Taking advantage of these methods and performing a high statistics simulation, we find a significant finite volume effect between the nucleon axial charges calculated on lattices with $(1.2\ \mathrm{fm})^3$ and $(2.4\ \mathrm{fm})^3$ volumes ($a \approx 0.15$ fm). On the large volume we find $g_A = 1.212 \pm 0.027(\mathrm{stat}) \pm 0.024(\mathrm{norm})$. The quoted systematic error is the dominant (known) one, corresponding to current renormalization. We discuss other possible remaining sources of error. This theoretical first principles calculation, which does not yet include isospin breaking effects, yields a value of g_A only a little bit below the experimental one, 1.2670 ± 0.0030.

DOI: 10.1103/PhysRevD.68.054509 PACS number(s): 11.15.Ha, 11.30.Rd, 12.38.Aw, 12.38.Gc

I. INTRODUCTION

The axial charge g_A of the nucleon, or more precisely its ratio to the vector charge g_V, appears to be a good test of our understanding of the structure of the nucleon. First of all, it is very accurately measured from neutron β decay, $g_A/g_V = 1.2670 \pm 0.0030$ [1].[1] And, among the nucleon form factors or moments of structure functions, it is technically the simplest from the point of view of a lattice QCD numerical calculation.

Four form factors appear in neutron β decay: the vector and induced tensor form factors from the vector current,

$$\langle p|V_\mu^+(x)|n\rangle = \overline{u}_p[\gamma_\mu g_V(q^2) - q_\lambda \sigma_{\lambda\mu} g_T(q^2)]u_n e^{-iq\cdot x}, \tag{1}$$

and the axial-vector and induced pseudoscalar form factors from the axial-vector current,

$$\langle p|A_\mu^+(x)|n\rangle = \overline{u}_p[\gamma_\mu\gamma_5 g_A(q^2) - iq_\mu\gamma_5 g_P(q^2)]u_n e^{-iq\cdot x}. \tag{2}$$

Here $q = p_n - p_p$ is the momentum transfer between the proton (p) and neutron (n). In the limit $|\vec{q}| \to 0$, the momentum transfer should be small because the mass difference of the neutron and proton is only about 1.3 MeV. This makes the limit $q^2 \to 0$, where the vector and axial-vector form factors dominate, a good approximation. Their values in this limit are called the vector and axial charges of the nucleon: $g_V = g_V(q^2=0)$ and $g_A = g_A(q^2=0)$. Experimentally, $g_V = \cos\theta_C$ (with the Cabibbo mixing angle θ_C), and $g_A = 1.2670(30) \times g_V$.

Since they are defined at zero momentum transfer, a naive expectation is that g_V and g_A are easier to calculate on the lattice than form factors which require nonzero momentum transfer. Despite this, quenched QCD lattice calculations with Wilson fermions at finite lattice cutoff ($a^{-1} \sim 2$ GeV) have underestimated g_A by about 20% [2–4] (see Table I for a summary of previous calculations). This suggests that systematic errors, which may arise from (1) the quenched approximation, (2) operator renormalization, (3) nonzero lattice spacing a and loss of chiral symmetry for Wilson and Kogut-Susskind fermions, and (4) finite volume, remain in the lattice calculation.

The first three errors have been addressed in previous calculations. The SESAM and LHPC Collaborations found that unquenching does not solve the problem as the estimated value g_A decreases by 5–10 % [5,6]. On the other hand, reducing the lattice spacing error seems to increase the value, but only by a small amount, $\lesssim$5% [7,8]. Perhaps more important is the calculation of the renormalization factor Z_A for the axial current. The one-loop perturbative renormalization factor, used in the case of Wilson fermions [2–6], was probably overestimated. The QCDSF-UKQCD Collaboration reported that the non-perturbatively calculated renormalization factor ($Z_A^{\mathrm{nonpert}} \sim 0.8$) is roughly 10% smaller than the one-loop one ($Z_A^{\mathrm{pert}} \sim 0.9$) in the case of the nonperturbatively $O(a)$ improved Wilson fermions [8] at $a^{-1} \sim 2$–3 GeV. Thus, the systematic error in the determination of the renormalization factor appears to be more important than the first two effects mentioned. The first two systematic errors listed

[1]Note that the Particle Data Group defines g_A to be negative because no assumption about the structure of the weak interaction is made. In this article, assuming the $V-A$ structure of the weak interaction, the axial form factor in Eq. (2) is defined to make g_A positive.

 ©2003 The American Physical Society

TABLE I. Previous lattice calculations with Wilson or $O(a)$ improved Wilson (clover) fermions. In general, g_A is significantly underestimated. Note that almost all volumes are small, most estimates use perturbative renormalization, and partially unquenching did not increase the value of g_A.

Type	Group	Fermion	$L^3\times N_t$	β	Volume	Statistics	$m_\pi L$	g_A	Reference
Quenched	KEK	Wilson	$16^3\times 20$	5.7	$(2.2\ \mathrm{fm})^3$	260	$\geqslant 5.9$	0.985(25)	[2]
	Kentucky	Wilson	$16^3\times 24$	6.0	$(1.5\ \mathrm{fm})^3$	24	$\geqslant 5.8$	1.20(11)	[3]
	DESY	Wilson	$16^3\times 32$	6.0	$(1.5\ \mathrm{fm})^3$	1000	$\geqslant 4.8$	1.07(9)	[4]
	LHPC-SESAM	Wilson	$16^3\times 32$	6.0	$(1.5\ \mathrm{fm})^3$	200	$\geqslant 4.8$	1.129(98)	[6]
	QCDSF	Wilson	$16^3\times 32$	6.0	$(1.5\ \mathrm{fm})^3$	$O(500)$		1.14(3)[a]	[7]
			$24^3\times 48$	6.2	$(1.6\ \mathrm{fm})^3$	$O(300)$			
			$32^3\times 48$	6.4	$(1.6\ \mathrm{fm})^3$	$O(100)$			
	QCDSF-UKQCD	Clover	$16^3\times 32$	6.0	$(1.5\ \mathrm{fm})^3$	$O(500)$		1.135(34)[a]	[8]
			$24^3\times 48$	6.2	$(1.6\ \mathrm{fm})^3$	$O(300)$			
			$32^3\times 48$	6.4	$(1.6\ \mathrm{fm})^3$	$O(100)$			
Full ($N_f=2$)	LHPC-SESAM	Wilson	$16^3\times 32$	5.5	$(1.7\ \mathrm{fm})^3$	100	$\geqslant 4.2$	0.914(106)	[6]
	SESAM	Wilson	$16^3\times 32$	5.6	$(1.5\ \mathrm{fm})^3$	200	$\geqslant 4.5$	0.907(20)	[5]

[a]Continuum extrapolated value.

above likely cannot resolve the issue that previous lattice calculations of g_A underestimate the experimental value.

The loss of chiral symmetry on the lattice is potentially significant. As is well known, $g_A/g_V=1$ in the absence of chiral symmetry breaking in QCD. Further, in the realistic case of spontaneously broken chiral symmetry, the ratio is still constrained by the axial Ward-Takahashi identity $\partial_\mu A^a_\mu(x)=2mP^a(x)$. The Goldberger-Treiman relation derives from the nucleon matrix elements of the currents on both sides of this identity in the soft pion limit [9]. We can easily understand the deviation of the ratio from unity in the context of the Gell-Mann–Oakes–Renner relation [10] which is also related to the axial Ward-Takahashi identity. Thus, the explicit breaking of chiral symmetry at nonzero lattice spacing a for Wilson fermions may induce significant errors which are removed only in the continuum limit.

In this work we use domain wall fermions (DWFs), a fermion discretization scheme with almost perfectly preserved chiral symmetry [11–13]. This scheme introduces a fictitious fifth dimension in addition to the four dimensions of space-time. In the limit where the fifth-dimensional extent L_s is taken to infinity, DWFs preserve the axial Ward Takahashi identity [14] at nonzero lattice spacing. With finite L_s the suppression of explicit chiral symmetry breaking is effectively exponential in quenched simulations if the gauge field is sufficiently smooth [15–20]. This is always true if the lattice spacing is sufficiently small. In low energy cases like the one investigated here, the small breaking of the symmetry at finite L_s is parametrized by a single universal ''residual mass'' parameter m_{res}, acting as an additive quark mass and defined from the axial Ward-Takahashi identity [18,21]. Furthermore, the DWF scheme greatly simplifies the nonperturbative determination of the renormalization of quark bilinear currents [22]. For example, the renormalization factors of local vector and axial-vector current operators should be equal, $Z_A=Z_V$ [22]. This means the ratio of the nucleon axial and vector charges calculated on the lattice directly yields the continuum value, i.e., it is not renormalized [23,24]. By employing the DWF scheme, the ambiguity in the renormalization of quark currents, which may be present and problematic in other fermion discretization schemes, is eliminated. We emphasize that the DWF calculation of the nucleon axial charge should not suffer from the systematic errors due to the operator renormalization and loss of chiral symmetry [23,24].

However, as is described in more detail in Sec. III, in our first DWF calculation with the single-plaquette Wilson gauge action at $\beta=6.0$ and lattice volume $16^3\times 32\times 16$ [which correspond to $a^{-1}\approx 2$ GeV and spatial volume $\sim(1.6\ \mathrm{fm})^3$], we found that g_A exhibits a fairly strong dependence on the quark mass [24]. A simple linear extrapolation of g_A to the chiral limit yielded a value that was almost a factor of 2 smaller than the experiment [24]. This implied the presence of a large finite volume effect. To our surprise, we found no systematic study of such an effect in the literature. Note also that there is no volume dependence in the naive quark model [25] nor in the MIT bag model [26]. In the former the ratio is determined by a simple spin-isospin algebra, and in the latter it arises from a simple overlap integral of the upper and lower components of the bag Dirac wave function.

To address the finite volume issue we need to have at the same time a sufficiently high lattice cutoff to preserve chiral symmetry reasonably well and at least two lattice volumes, preferably ones that are large compared to the charge radius of the proton. The Wilson gauge action will not work for this purpose since the chiral symmetry of DWFs in the quenched case degrades rapidly as lattice spacing a increases, while the computational cost necessitated by a very large lattice volume would be prohibitive. Fortunately, various ''renormalization-group-inspired'' improved gauge actions preserve the chiral symmetry of the DWFs well while not demanding a large cutoff [19,20]. Thus both requirements, chiral symmetry and large physical volume, can be met at reasonable computational cost. Of the relatively well-established candidates in this class of improved gauge actions, we choose the ''doubly blocked Wilson 2'' (DBW2) action [20,27].

The rest of this paper is organized as follows. In Sec. II the lattice method for calculating g_A/g_V is described. In Sec. III, the numerical results obtained for both Wilson and DBW2 actions are described in detail. Finally, in Sec. IV we summarize the present work and discuss future directions.

II. GENERAL ANALYTIC FRAMEWORK

A. The vector and axial charges

As mentioned in the Introduction, four form factors are needed to describe neutron β decay: the vector and induced tensor form factors for the vector current,

$$\langle p|V_\mu^+(0)|n\rangle=\overline{u}_p[\,\gamma_\mu g_V(q^2)-q_\lambda\sigma_{\lambda\mu}g_T(q^2)]u_n\,, \quad (3)$$

and the axial and induced pseudoscalar for the axial current,

$$\langle p|A_\mu^+(0)|n\rangle=\overline{u}_p[\,\gamma_\mu\gamma_5 g_A(q^2)-iq_\mu\gamma_5 g_P(q^2)]u_n\,. \quad (4)$$

The right hand side of each is the most general form consistent with Lorentz covariance. The momentum transfer $q=p_n-p_p$ becomes very small in the forward limit because of the small mass difference between the neutron and proton. In the limit $q^2\to 0$, which we take in this work, the vector and axial form factors dominate the matrix elements. We are neglecting the mass difference of the neutron and proton, and hence that of up and down quarks (we also neglect the electromagnetic mass difference). For zero quark mass $m=m_u=m_d=0$ the action is symmetric under global chiral SU(2) $\times$SU(2) flavor rotations acting on the quark fields. If $m\neq 0$, the symmetry is broken down to the vector (flavor) SU(2) subgroup, and the associated vector charge g_V is still conserved ($g_V=1$). This situation is sometimes called CVC, conserved vector current. In the real world even this symmetry is softly broken by the small mass difference between up and down quarks, m_u-m_d. The explicit violation of the axial-vector symmetry by nonzero quark mass is sometimes called PCAC, or partially conserved axial-vector current. As is well known the axial SU(2) symmetry is also spontaneously broken. Thus, the axial charge may in general deviate from unity, $g_A\neq 1$.

If the vector symmetry is preserved, a simple exercise in SU(2) Lie algebra leads to the following (see the Appendix):

$$\langle p|A_\mu^+|n\rangle=2\langle p|A_\mu^3|p\rangle=\langle p|A_\mu^u|p\rangle-\langle p|A_\mu^d|p\rangle, \quad (5)$$

where $A_\mu^+=\overline{u}\gamma_\mu\gamma_5 d$, $A_\mu^3=(1/2)(A_\mu^u-A_\mu^d)$, $A_\mu^u=\overline{u}\gamma_\mu\gamma_5 u$, and $A_\mu^d=\overline{d}\gamma_\mu\gamma_5 d$. u and d stand for the up and down quark fields. A similar relation holds for the vector case,

$$\langle p|V_\mu^+|n\rangle=2\langle p|V_\mu^3|p\rangle=\langle p|V_\mu^u|p\rangle-\langle p|V_\mu^d|p\rangle, \quad (6)$$

where $V_\mu^+=\overline{u}\gamma_\mu d$, $V_\mu^3=(1/2)(V_\mu^u-V_\mu^d)$, $V_\mu^u=\overline{u}\gamma_\mu u$, and $V_\mu^d=\overline{d}\gamma_\mu d$. The isovector vector charge g_V and the isovector axial charge g_A are defined by the strength of the right-hand sides of Eqs. (5) and (6) in the forward limit ($q^2\to 0$). In addition, the polarized quark distributions in the proton for each flavor f, $\Delta\psi_f$, are defined by the forward matrix elements of the flavor axial-vector currents A_μ^f:

$$\langle k,s|\overline{\psi}_f\gamma_\mu\gamma_5\psi_f|k,s\rangle=\Delta\psi_f\overline{u}_p(k,s)\,\gamma_\mu\gamma_5 u_p(k,s), \quad (7)$$

where k and s are the proton four-momentum and polarization. From CVC we find the relation $g_A=\Delta u-\Delta d$.

Now consider the conserved electromagnetic current $j_\mu^{\text{e.m.}}$ expressed in terms of the flavor vector currents V_μ^f:

$$j_\mu^{\text{e.m.}}=\sum_f Q_f V_\mu^f=\frac{2}{3}V_\mu^u-\frac{1}{3}V_\mu^d+\cdots. \quad (8)$$

Here Q_f denotes the charge (in units of proton charge e) for a quark of flavor f, and the ellipsis denotes possible flavors of heavier quarks which we henceforth ignore. Since the corresponding electromagnetic U(1) gauge symmetry assures conservation of electric charge, for the neutron we find

$$\lim_{q^2\to 0}\langle n|j_\mu^{\text{e.m.}}|n\rangle=0. \quad (9)$$

It follows that

$$\lim_{q^2\to 0}\langle n|V_\mu^d|n\rangle=2\times\lim_{q^2\to 0}\langle n|V_\mu^u|n\rangle. \quad (10)$$

On the other hand, under the assumption of CVC we have the following:

$$\langle n|V_\mu^u|n\rangle=\langle p|V_\mu^d|p\rangle, \quad (11)$$

$$\langle n|V_\mu^d|n\rangle=\langle p|V_\mu^u|p\rangle. \quad (12)$$

Thus we reach the following relation:

$$\lim_{q^2\to 0}\langle p|j_\mu^{\text{e.m.}}|p\rangle=\lim_{q^2\to 0}\langle p|V_\mu^d|p\rangle=\lim_{q^2\to 0}\langle p|V_\mu^u-V_\mu^d|p\rangle. \quad (13)$$

Likewise, it follows that the vector charge g_V must be unity (in units of $\cos\theta_C$ and e) under CVC since the proton electric charge is unity. As already mentioned, we expect a very small breaking from CVC because of the physical up and down quark mass difference. In the axial case, we expect nonconservation of g_A due to the small but nonzero up and down quark masses as well as the spontaneous breakdown of chiral symmetry.

B. Nucleon matrix elements

In this subsection we describe our method of lattice numerical calculation of the axial and vector charges of the nucleon. Hadronic matrix elements calculated on the lattice are determined from ratios of the relevant three-point to two-point correlation functions. Since the charges are defined at zero-momentum transfer, we do not have to introduce nonzero momentum projection for the nucleon source and sink for these correlation functions, nor for the current insertion. On the other hand since we are dealing with a spin-1/2 baryon, both correlation functions possess nontrivial Dirac spinor structure, so appropriate projections are necessary.

The zero-momentum two-point function for the nucleon is given by the sum over all spatial coordinates $\vec{x}$,

$$\langle \mathcal{N}(t)\overline{\mathcal{N}}(0)\rangle_{\alpha\beta} = \sum_{\vec{x}} \langle 0|\mathcal{N}_\alpha(\vec{x},t)\overline{\mathcal{N}}_\beta(\vec{0},0)|0\rangle, \quad (14)$$

where $\mathcal{N}(\vec{x},t)$ can be any operator with the same quantum numbers as the nucleon, namely, unit baryon number, $J^P = (1/2)^+$, and isospin doublet. α and β denote Dirac indices. Color and flavor indices are suppressed in the following unless noted otherwise. The two-point correlation has the asymptotic form

$$\langle \mathcal{N}(t)\overline{\mathcal{N}}(0)\rangle_{\alpha\beta} = \frac{A_N}{2}[1+\mathrm{sgn}(t)\gamma_4]_{\alpha\beta} e^{-M_N|t|} \quad (15)$$

at large Euclidean time t. Here M_N denotes the ground state mass of the nucleon. The amplitude A_N is defined as $\langle 0|\mathcal{N}(0)|N\rangle = \sqrt{A_N} u_N$. In general, the baryon two-point function receives contributions from both positive- and negative-parity states. By taking the trace with a projection operator $P_+ = (1+\gamma_4)/2$, we eliminate contributions from the opposite-parity state in the forward time direction. Details of the parity projection are described in [28]. Let us abbreviate the notation for the two-point function of the particle contribution from the desired (positive-parity) state as

$$G_N(t) = \frac{1}{4}\mathrm{Tr}[P_+ \langle \mathcal{N}(t)\overline{\mathcal{N}}(0)\rangle]. \quad (16)$$

The factor of 1/4 is our choice of normalization. At large t this asymptotically approaches a simple exponential,

$$G_N(t) \sim \exp(-M_N t). \quad (17)$$

For the proton, a standard choice for the interpolating operator is

$$\mathcal{N}(x) = \varepsilon_{abc}[u_a^T(x) C\gamma_5 d_b(x)] u_c(x) \quad (18)$$

where C is the charge conjugation matrix defined as $C = \gamma_4\gamma_2$, abc the color indices, and u and d the up and down quark fields.

Next, let us define the zero-momentum three-point correlation function for quark bilinears, $\mathcal{O}_\Gamma^{(f)}(x) = \overline{\psi}_f(x)\Gamma\psi_f(x)$:

$$\langle \mathcal{N}(t)\mathcal{O}_\Gamma(t')\overline{\mathcal{N}}(0)\rangle_{\alpha\beta} = \sum_{\vec{x}}\sum_{\vec{x}'} \langle 0|T\{\mathcal{N}_\alpha(\vec{x},t)\mathcal{O}_\Gamma(\vec{x}',t')\overline{\mathcal{N}}_\beta(\vec{0},0)\}|0\rangle, \quad (19)$$

where Γ is any of the 16 possible matrices in the Clifford algebra defined by the Dirac gamma matrices. When $t \gg t' \gg 0$, the particle contribution of the zero-momentum three-point function becomes

$$\langle \mathcal{N}(t)\mathcal{O}_\Gamma(t')\overline{\mathcal{N}}(0)\rangle_{\alpha\beta} \to A_N \lim_{q^2\to 0} g_\Gamma(q^2)\exp(-M_N t)(P_+\Gamma P_+)_{\alpha\beta}. \quad (20)$$

Note two important points: first, the three-point function vanishes for Γ other than 1, γ_4, $\gamma_i\gamma_5$ $(i=1,2,3)$, and σ_{ij} $(i,j=1,2,3)$ because $P_+\Gamma P_+ = 0$ for Γ's that do not commute with γ_4. Second, the right-hand side of the above asymptotic formula does not depend on the insertion point of the operator $\mathcal{O}_\Gamma$. Any t' dependence arises from excited state contamination, i.e., away from the asymptotic regime.

In this paper, we calculate the isovector (quark-flavored) vector charge g_V and the isovector axial charge g_A of the nucleon. We define the spin projected three-point function for the relevant components of the vector current $V_\mu^f = \overline{\psi}_f\gamma_\mu\psi_f$ and the axial current $A_\mu^f = \overline{\psi}_f\gamma_\mu\gamma_5\psi_f$ by taking traces with the projection operators $P_\Gamma = P_+\Gamma^{-1}$:

$$G_V^f(t,t') = \frac{1}{4}\mathrm{Tr}[P_V\langle \mathcal{N}(t)V_4^f(t')\overline{\mathcal{N}}(0)\rangle], \quad (21)$$

$$G_A^f(t,t') = \frac{1}{4}\mathrm{Tr}[P_{A_i}\langle \mathcal{N}(t)A_i^f(t')\overline{\mathcal{N}}(0)\rangle], \quad (22)$$

where $P_V = P_+$ and $P_{A_i} = P_+\gamma_i\gamma_5$ $(i=1,2,3)$. In order to extract g_Γ (Γ is either V or A) on the lattice, we have to identify a plateau in the ratio of the three- and two-point functions,

$$g_\Gamma^{\mathrm{lattice}} = \frac{G_\Gamma^u(t,t') - G_\Gamma^d(t,t')}{G_N(t)} \quad (23)$$

in the range of $t > t'$ with fixed $t = t_{\mathrm{sink}} - t_{\mathrm{source}}$.

In general, lattice operators receive finite renormalizations relative to their continuum counterparts since the exact symmetries of the continuum are usually realized only in the continuum limit $a \to 0$. Thus

$$g_\Gamma^{\mathrm{ren}} = Z_\Gamma g_\Gamma^{\mathrm{lattice}} \quad (24)$$

requires some independent estimation of Z_Γ, the renormalization of the quark bilinear currents,

$$[\overline{\psi}\Gamma\psi]^{\mathrm{ren}} = Z_\Gamma[\overline{\psi}\Gamma\psi]^{\mathrm{lattice}} \quad (25)$$

Since DWFs possess full chiral symmetry at nonzero lattice spacing, a lattice conserved vector current $\mathcal{V}_\mu$ and partially conserved axial-vector current $\mathcal{A}_\mu$ which receive no lattice renormalization can be defined, namely, $Z_\mathcal{V} = Z_\mathcal{A} = 1$ [14]. However these conserved currents are point split and require sums over the extra fifth dimension of the DWF, so they are somewhat costly to work with in practice. Alternatively the local currents V_μ and A_μ, which are naive transcriptions of the continuum operators, are easier to deal with but receive a

finite renormalization since they do not correspond to an exact symmetry of the action. However, the Ward-Takahashi identity satisfied by both types of currents is enough to ensure that the lattice renormalizations of the local currents are equal, $Z_V = Z_A$, up to terms of order $O(a^2)$ in the chiral limit and neglecting explicit chiral symmetry breaking for the DWF at finite L_s,

$$\left(\frac{g_A}{g_V}\right)^{\text{ren}} = \left(\frac{G_A^\mu(t,t') - G_A^d(t,t')}{G_V^u(t,t') - G_V^d(t,t')}\right)^{\text{lattice}} + \mathcal{O}(a^2). \quad (26)$$

Note that the vector charge computed from the local current provides an independent estimate of Z_V since the renormalization of an operator does not depend on any particular matrix element and the renormalized, or physical, value of g_V is 1 by CVC:

$$Z_V = \frac{G_N(t)}{G_V^u(t,t') - G_V^d(t,t')}. \quad (27)$$

Comparison of Z_V thus obtained to the value of Z_A from the relation [18]

$$\langle \mathcal{A}_\mu(t)[\bar{\psi}\gamma_5\psi](0)\rangle = Z_A \langle A_\mu(t)[\bar{\psi}\gamma_5\psi](0)\rangle \quad (28)$$

yields an estimate of the $O(a^2)$ systematic errors arising from the method described here. These are discussed in Sec. III.

Next we describe the particular interpolating operators, or quark sources and sinks, used to calculate lattice correlation functions. In our earlier work we used so-called wall-wall correlation functions constructed with quark sources generated from a unit source at each spatial site on a fixed source time slice and summed over all spatial sites at the sink time slice. Since the wall source or sink is gauge variant, we fix to the Coulomb gauge. Later we switched to wall-point correlation functions since they yield smaller statistical errors. For three-point functions this approach is implemented with a sequential source. We discuss both types of correlation functions in turn.

First, we introduce the forward quark propagators from a wall source to a wall sink and from a wall source to a point sink, which may be written with the gauge fixed point-to-point quark propagator S_{PP}:

$$S_{WW}(t,t')^{ab}_{\alpha\beta} = \sum_{\vec{x}} S_{PW}(\vec{x},t;t')^{ab}_{\alpha\beta}, \quad (29)$$

$$S_{PW}(\vec{x},t;t')^{ab}_{\alpha\beta} = \sum_{\vec{y}} S_{PP}(\vec{x},t;\vec{y},t')^{ab}_{\alpha\beta} \quad (30)$$

where the subscripts and superscripts denote Dirac and color indices, respectively. The quark three-point function resulting from insertion of the quark bilinear operator $\bar{\psi}_f \Gamma \psi_f$ is defined as

$$\begin{aligned}\mathcal{S}_\Gamma(t,t',t'')^{ab}_{\alpha\beta} &= \sum_{\vec{x},\vec{y},\vec{z}} S_{PP}(\vec{x},t;\vec{y},t')^{ac}_{\alpha\gamma}(\Gamma)_{\gamma\gamma'} S_{PP}(\vec{y},t';\vec{z},t'')^{cb}_{\gamma'\beta} \\ &= \sum_{\vec{z}} \gamma_{5,\gamma\delta'} S^*_{PW}(\vec{x},t';t)^{ca}_{\delta'\delta} \gamma_{5,\delta\alpha}(\Gamma)_{\gamma\gamma'} S_{PW}(\vec{x},t';t'')^{cb}_{\gamma'\beta}\end{aligned} \quad (31)$$

where the second equality results from $S_{PP}(\vec{x},t;\vec{y},t') = \gamma_5 S^\dagger_{PP}(\vec{y},t';\vec{x},t)\gamma_5$. Thus, $\mathcal{S}_\Gamma(t,t',t'')$ is constructed by combining wall-to-point quark propagators generated from two different source time slices t and t'' at either end of the lattice with the operator inserted in between them.

The two-point function for the nucleon in Eq. (14) is expressed in terms of quark propagators as

$$\begin{aligned}\langle \mathcal{N}(t)\bar{\mathcal{N}}(0)\rangle_{\alpha\alpha'} = \varepsilon_{abc}\varepsilon_{a'b'c'}(C\gamma_5)_{\beta\gamma} S^{(d)}_{WW}(t,0)^{cc'}_{\gamma\gamma'}(C\gamma_5)_{\beta'\gamma'} \\ \times [S^{(u)}_{WW}(t,0)^{aa'}_{\alpha\alpha'} S^{(u)}_{WW}(t,0)^{bb'}_{\beta\beta'} + S^{(u)}_{WW}(t,0)^{aa'}_{\alpha\beta'} S^{(u)}_{WW}(t,0)^{bb'}_{\beta\alpha'}].\end{aligned} \quad (32)$$

Following Ref. [29], the three-point function in Eq. (19) is easily obtained from the two-point function by replacing the ordinary quark propagator by the operator inserted one, $\mathcal{S}_\Gamma(t,t',0)$. Inserting the d and u quark currents, we obtain

$$\begin{aligned}\langle \mathcal{N}(t)\mathcal{O}^{(d)}_\Gamma(t')\bar{\mathcal{N}}(0)\rangle_{\alpha\alpha'} = \varepsilon_{abc}\varepsilon_{a'b'c'}(C\gamma_5)_{\beta\gamma}\mathcal{S}^{(d)}_\Gamma(t,t',0)^{cc'}_{\gamma\gamma'}(C\gamma_5)_{\beta'\gamma'} \\ \times [S^{(u)}_{WW}(t,0)^{aa'}_{\alpha\alpha'} S^{(u)}_{WW}(t,0)^{bb'}_{\beta\beta'} + S^{(u)}_{WW}(t,0)^{aa'}_{\alpha\beta'} S^{(u)}_{WW}(t,0)^{bb'}_{\beta\alpha'}]\end{aligned} \quad (33)$$

and

$$\begin{aligned}\langle \mathcal{N}(t)\mathcal{O}^{(u)}_\Gamma(t')\bar{\mathcal{N}}(0)\rangle_{\alpha\alpha'} = \varepsilon_{abc}\varepsilon_{a'b'c'}(C\gamma_5)_{\beta\gamma} S^{(d)}_{WW}(t,0)^{cc'}_{\gamma\gamma'}(C\gamma_5)_{\beta'\gamma'} \\ \times [\mathcal{S}^{(u)}_\Gamma(t,t',0)^{aa'}_{\alpha\alpha'} S^{(u)}_{WW}(t,0)^{bb'}_{\beta\beta'} + \mathcal{S}^{(u)}_\Gamma(t,t',0)^{aa'}_{\alpha\beta'} S^{(u)}_{WW}(t,0)^{bb'}_{\beta\alpha'} + S^{(u)}_{WW}(t,0)^{aa'}_{\alpha\alpha'} \mathcal{S}^{(u)}_\Gamma(t,t',0)^{bb'}_{\beta\beta'} \\ + S^{(u)}_{WW}(t,0)^{aa'}_{\alpha\beta'} \mathcal{S}^{(u)}_\Gamma(t,t',0)^{bb'}_{\beta\alpha'}].\end{aligned} \quad (34)$$

The nucleon three-point function is the sum of the up and down quark contributions. The spin projected three-point functions are obtained from Eqs. (21) and (22).

To enhance the signal, a point sink is more desirable than an extended sink. The wall-point type of three-point functions is implemented using the so-called sequential source method [6,30,31]. In addition we use a box source instead of a wall source to enhance the coupling to the ground state:

$$S_{PB}(\vec{x},t;t')^{ab}_{\alpha\beta}=\sum_{0\leq\vec{y}\leq B} S_{PP}(\vec{x};t;\vec{y},t')^{ab}_{\alpha\beta}. \tag{35}$$

We adjust the box size B to about 1 fm. In describing the construction of the sequential source, it is convenient to introduce the ''diquark'' propagators:

$$\mathcal{D}_{\alpha\alpha'}(\vec{y},t;0)^{a'a}_{\beta'\beta}=\varepsilon_{abc}\varepsilon_{a'b'c'}(C\gamma_5)_{\delta\beta}(C\gamma_5)_{\delta'\beta'} \times[S^{(u)}_{PB}(\vec{y},t;0)^{bb'}_{\beta\beta'}S^{(u)}_{PB}(\vec{y},t;0)^{cc'}_{\gamma\gamma'}+S^{(u)}_{PB}(\vec{y},t;0)^{bb'}_{\gamma\beta'}S^{(u)}_{PB}(\vec{y},t;0)^{cc'}_{\beta\gamma'}] \tag{36}$$

and

$$\mathcal{U}_{\alpha\alpha'}(\vec{y},t;0)^{b'b}_{\beta'\beta}=\varepsilon_{abc}\varepsilon_{a'b'c'}S^{(d)}_{PB}(\vec{y},t;0)^{cc'}_{\gamma\gamma'} \times[(C\gamma_5)_{\beta\gamma}(C\gamma_5)_{\beta'\gamma'}S^{(u)}_{PB}(\vec{y},t;0)^{aa'}_{\alpha\alpha'}+(C\gamma_5)_{\delta\gamma}(C\gamma_5)_{\delta'\gamma'}S^{(u)}_{PB}(\vec{y},t;0)^{aa'}_{\delta\delta'}\delta_{\alpha\beta}\delta_{\alpha'\beta'} +(C\gamma_5)_{\beta\gamma}(C\gamma_5)_{\delta'\gamma'}S^{(u)}_{PB}(\vec{y},t;0)^{aa'}_{\alpha\delta'}\delta_{\alpha'\beta'}+(C\gamma_5)_{\delta\gamma}(C\gamma_5)_{\beta'\gamma'}S^{(u)}_{PB}(\vec{y},t;0)^{aa'}_{\delta\alpha'}\delta_{\alpha\beta}]. \tag{37}$$

The ''down diquark'' ($\mathcal{D}$) and ''up diquark'' ($\mathcal{U}$) are defined by the down quark removed propagator and one up quark removed propagator from the nucleon two-point function. Now using the diquark we can reconstruct the point-to-wall type of the nucleon two-point function as

$$\langle\mathcal{N}(t)\bar{\mathcal{N}}(0)\rangle_{\alpha\alpha'}=\sum_{\vec{y}}\mathcal{D}_{\alpha\alpha'}(\vec{y},t;0)^{ba}_{\beta'\beta}S^{(d)}_{PB}(\vec{y},t;0)^{ab}_{\beta\beta'}=\frac{1}{2}\sum_{\vec{y}}\mathcal{U}_{\alpha\alpha'}(\vec{y},t;0)^{ba}_{\beta'\beta}S^{(u)}_{PB}(\vec{y},t;0)^{ab}_{\beta\beta'}. \tag{38}$$

In terms of the diquarks the three-point functions of an arbitrary quark bilinear operator $\bar{\psi}_f\Gamma\psi_f$ at a location $(\vec{z},t')$ can be written for the down quark as

$$\langle\mathcal{N}(t)\mathcal{O}^{(d)}_{\Gamma}(t')\bar{\mathcal{N}}(0)\rangle_{\alpha\alpha'}=\sum_{\vec{y},\vec{z}}\mathcal{D}_{\alpha\alpha'}(\vec{y},t;0)^{a'a}_{\beta'\beta}S^{(d)}_{PP}(\vec{y},t;\vec{z},t')^{ae}_{\beta\delta}(\Gamma)_{\delta\delta'}S^{(d)}_{PB}(\vec{z},t';0)^{ea'}_{\delta'\beta'} \tag{39}$$

and for the up quark as

$$\langle\mathcal{N}(t)\mathcal{O}^{(u)}_{\Gamma}(t')\bar{\mathcal{N}}(0)\rangle_{\alpha\alpha'}=\sum_{\vec{y},\vec{z}}\mathcal{U}_{\alpha\alpha'}(\vec{y},t;0)^{b'b}_{\beta'\beta}S^{(u)}_{PP}(\vec{y},t;\vec{z},t')^{be}_{\beta\delta}(\Gamma)_{\delta\delta'}S^{(u)}_{PB}(\vec{z},t';0)^{eb'}_{\delta'\beta'}. \tag{40}$$

For the construction of the three-point functions we need the backward propagators from the sink point $(\vec{y},t)$ to the operator insertion point $(\vec{z},t')$. However, it is highly expensive to prepare the required point-to-point quark propagators from all points $(\vec{y},t)$. This difficulty is easily circumvented by directly computing the generalized quark propagators $\mathcal{D}_{\alpha\alpha'}(\vec{y},t;0)S^{(d)}_{PP}(\vec{y},t;\vec{z},t')$ and $\mathcal{U}_{\alpha\alpha'}(\vec{y},t;0)S^{(u)}_{PP}(\vec{y},t;\vec{z},t')$ with the sequential source method.

Before describing details of the sequential source propagator, we should apply the spin projection P_Γ to diquarks in order to reduce the cost from having to calculate all 4×4 matrices for external spinor indices (α,α'). In this article, we need only two kinds of spin projections, i.e., P_V and P_{A_3}, so that it reduces the amount of calculations by a factor of 8 in comparison with the unprojected case. The spin projected source for a down quark insertion is

$$\mathbf{\Phi}_d(\vec{y},t;0)^{ab}_{\alpha\beta}=\frac{1}{4}\mathcal{D}_{\gamma\gamma'}(\vec{y},t;0)^{ab}_{\alpha\beta}(P_\Gamma)_{\gamma'\gamma}, \tag{41}$$

and for the up quark

$$\mathbf{\Phi}_u(\vec{y},t;0)^{ab}_{\alpha\beta}=\frac{1}{4}\mathcal{U}_{\gamma\gamma'}(\vec{y},t;0)^{ab}_{\alpha\beta}(P_\Gamma)_{\gamma'\gamma}. \tag{42}$$

Finally, the sequential source down quark propagator is

TABLE II. Simulation parameters for each action and each volume studied in this work.

Gauge action	β	$L^3\times N_t$	L_s	M_5	Volume
Wilson	6.0	$16^3\times32$	16	1.8	$(1.6\text{ fm})^3$
DBW2	0.87	$16^3\times32$	16	1.8	$(2.4\text{ fm})^3$
		$8^3\times24$	16	1.8	$(1.2\text{ fm})^3$

$$\mathbf{\Sigma}_d(t,0;\vec{z},t')^{ab}_{\alpha\beta}=\left(\sum_{\vec{y},t''}\gamma_{5,\beta\gamma}S^{(d)}_{PP}(\vec{z},t';\vec{y},t)^{be}_{\gamma\gamma'}\gamma_{5,\gamma'\delta}\delta_{t'',t}\mathbf{\Phi}^*_d(\vec{y},t'';0)^{ae}_{\alpha\delta}\right)^*, \tag{43}$$

and the sequential source up quark propagator is

$$\mathbf{\Sigma}_u(t,0;\vec{z},t')^{ab}_{\alpha\beta}=\left(\sum_{\vec{y},t''}\gamma_{5,\beta\gamma}S^{(u)}_{PP}(\vec{z},t';\vec{y},t)^{be}_{\gamma\gamma'}\gamma_{5,\gamma'\delta}\delta_{t'',t}\mathbf{\Phi}^*_u(\vec{y},t'';0)^{ae}_{\alpha\delta}\right)^*, \tag{44}$$

which may be calculated by solving the matrix equations

$$\sum_{\vec{x},t''}\mathbf{\Sigma}_f(t,0;\vec{x},t'')^{ab}_{\alpha\beta}\mathcal{M}^{\dagger}(\vec{x},t'';\vec{z},t')^{bc}_{\beta\gamma}=\delta_{tt'}\mathbf{\Phi}_f(\vec{z},t';0)^{ac}_{\alpha\gamma}, \tag{45}$$

where $\mathcal{M}$ is the Dirac matrix. Consequently, in terms of the sequential source propagator, the spin projected three-point function for the down quark is written

$$G^d_\Gamma(t,t')=\sum_{\vec{z}}\mathbf{\Sigma}_d(t,0;\vec{z},t')^{ab}_{\alpha\beta}(\Gamma)_{\beta\gamma}S^{(d)}_{PB}(\vec{z},t';0)^{ba}_{\gamma\alpha} \tag{46}$$

and for the up quark is

$$G^u_\Gamma(t,t')=\sum_{\vec{z}}\mathbf{\Sigma}_u(t,0;\vec{z},t')^{ab}_{\alpha\beta}(\Gamma)_{\beta\gamma}S^{(u)}_{PB}(\vec{z},t';0)^{ba}_{\gamma\alpha}. \tag{47}$$

In the case of keeping the up and down quark masses equal, the total cost for computing the sequential source propagator is a factor of 2 over the cost for wall-wall correlation functions. However, the resulting box-point correlation functions yield smaller statistical errors.

III. NUMERICAL RESULTS

We have performed quenched lattice calculations using two different gauge actions, the standard Wilson and the improved DBW2 [27]. Details and some relevant results of both simulations are summarized in Tables II, III, and IV. We describe the nucleon matrix element results for each one separately, then compare them and draw some conclusions.

A. Wilson gauge action results at $\beta=6.0$

We have performed a quenched simulation on a $16^3\times 32$ lattice with the standard single-plaquette Wilson action at $\beta=6/g^2=6.0$ which corresponds to a lattice cutoff of $a^{-1}=1.922$ GeV set by the ρ mass [18]. Quark propagators were generated with four bare masses $m_f=0.02$, 0.03, 0.04, and 0.05, using DWFs with $L_s=16$ and $M_5=1.8$. The nucleon matrix elements were averaged on a set of 400 gauge con-

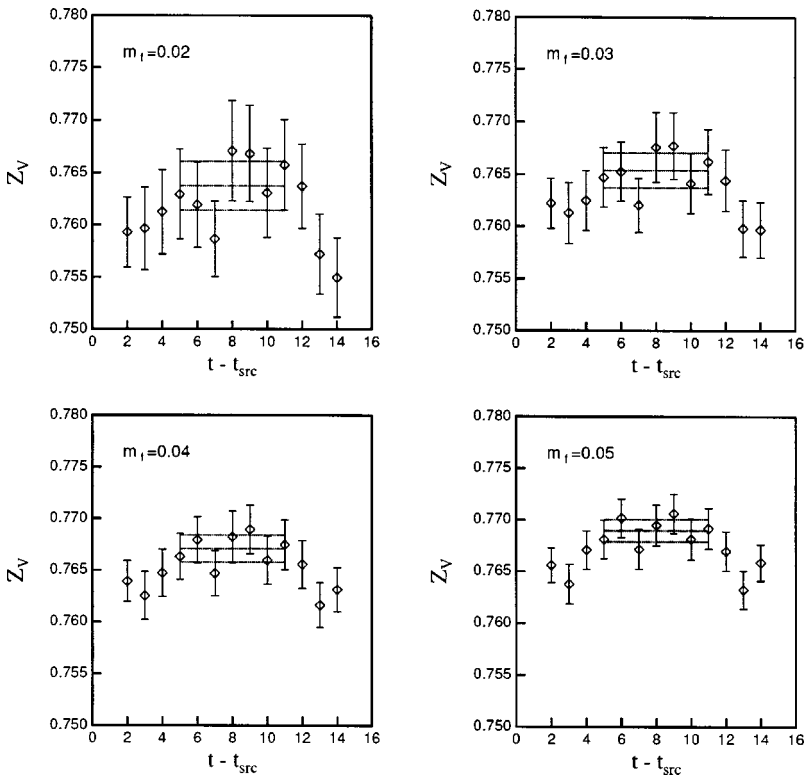

FIG. 1. $Z_V=1/g_V^{\text{lattice}}$, Wilson gauge action, as a function of the current insertion time slice. Note the very fine scale. A good plateau for each quark mass is observed in the middle range between the source and sink. The lines denote central values and statistical errors from constant fits over the plateaus.

TABLE III. More parameters for each action and each volume.

Gauge action (β)	$L^3\times N_t$	Quark mass values	Statistics (type)	$m_\pi L$
Wilson (6.0)	$16^3\times 32$	0.02, 0.03, 0.04, 0.05	400 (wall)	$\geqslant$4.3
DBW2 (0.87)	$16^3\times 32$	0.02, 0.04, 0.06, 0.08, 0.10	416 (sequential)	$\geqslant$4.8
	$8^3\times 24$	0.04, 0.06, 0.08, 0.10	400 (sequential)	$\geqslant$3.4
		0.04, 0.06, 0.08, 0.10	400 (wall)	

figurations. Hadron masses computed on these lattices are tabulated in Table V. Preliminary results for the nucleon charges were first reported in [24].

We calculated wall-source quark propagators on each Coulomb-gauge-fixed configuration for both periodic and antiperiodic boundary conditions in the time direction for the quarks. A simple linear combination of these propagators then yields a forward (or backward) in time propagator. To compute the correlation functions, we employed the wall-wall method described in the previous section with source locations fixed at $t_{\rm src}=5$ and $t'_{\rm src}=21$.

In Fig. 1 we show the dependence of the vector renormalization $Z_V=1/g_V^{\rm lattice}$ on the location of the current insertion. A good plateau is observed in the middle region between the source and sink. The quoted errors are estimated by a single elimination jackknife method. The lines represent the average value and statistical error in the time-slice range $5\leqslant t-t_{\rm src}\leqslant 11$. The mass dependence of Z_V is rather mild as seen in Fig. 2 and given in Table VI. The values 0.7601(31) for a linear fit and 0.7610(52) for a quadratic fit at $m_f=0$ agree well with $Z_A=0.7555(3)$ [18], which was obtained from a calculation of meson two-point correlation functions. The discrepancy $\Delta Z\equiv|1-Z_A/Z_V|$ is less than 0.6% which implies that the $O(a^2)$ error that remains after taking the $m_f\rightarrow 0$ limit is quite small.

As is seen in Fig. 3, plateaus are evident for the spin-dependent distribution functions Δu and Δd in the range $5\leqslant t-t_{\rm src}\leqslant 11$. Thus, we compute the charge ratios $(g_A/g_V)^{\rm lattice}$ at each m_f by taking a weighted average over this time-slice range. In Fig. 4 a strong dependence on m_f appears. A simple linear extrapolation to $m_f=0$ yields 0.812(112), which is roughly 2/3 of the experimental value. However, a simple linear ansatz may not describe the data, which show increasing downward curvature for lighter quark mass (note that the points are correlated in this quenched calculation since they are computed on the same gauge configurations). In general chiral logarithms may appear and were considered. In fact, the data are not compelling for such terms, arising in either quenched or full chiral perturbation theory [32,33]. The results for each mass are reproduced in Table VI.

This implies the existence of other systematic errors. As was mentioned in the introduction, a large systematic error in previous lattice calculations of g_A came from the determination of the renormalization constant Z_A. As shown above using DWFs, the value of g_A is determined in a fully nonperturbative way, with or without explicit renormalization. The systematic error stemming from the incomplete cancellation of renormalization factors in the ratio is less than 1% as we saw by comparing $Z_V=1/g_V^{\rm lattice}$ and Z_A calculated from meson two-point functions. In addition, comparing the chirally extrapolated values of $(g_A/g_V)^{\rm lattice}$ and $Z_A g_A^{\rm lattice}$ leads to an even smaller error, although it relies on the linear extrapolation, which was not very compelling. Another possible systematic error is the contribution of excited states, the presence or absence of which was checked by slightly enlarging the separation between wall sources $t_{\rm src}$ $(=5)$ and $t_{\rm sink}$ $(=27)$. While the larger separation induces more noise in the signal, the central value of g_A is essentially unchanged for each quark mass; thus we cannot detect a systematic effect outside of the statistical errors. Still, this source of error appears to be small.

Detailed detection of quenching effects such as quenched chiral logarithms, unsuppressed fermionic zero modes, and the absence of the physical pion cloud is beyond our scope at present since these require very light quark masses and correspondingly large statistics. Thus, by a process of elimination we are led to focus on finite volume effects which we discuss in the next section. The volume employed for the calculations in this subsection is roughly $(1.5–1.6\ {\rm fm})^3$ which can barely accommodate a proton with mean square radius estimated to be about 0.8 fm [1].

B. DBW2 action results at $\beta=0.87$

To determine g_A in a large physical volume, say $\gtrsim(2\ {\rm fm})^3$, we have performed a DWF simulation on a lattice with larger spacing. In general, it is difficult to maintain the good chiral properties of DWFs as a increases at fixed L_s, especially with the Wilson gauge action [18,19]. It has been shown that the Iwasaki gauge action enables studies of quenched DWFs with smaller L_s than the Wilson gauge ac-

TABLE IV. The residual mass $m_{\rm res}$, hadron masses, inverse lattice spacing (a_ρ^{-1}, set by the ρ meson mass), and the renormalization factor of the axial-vector current (Z_A). The ρ meson mass and the nucleon mass are given in the chiral limit in each case.

Gauge action (β)	M_5	L_s	$m_{\rm res}$	m_ρ	m_N	a_ρ^{-1} (GeV)	Z_A	Reference
Wilson (6.0)	1.8	16	$1.24(5)\times 10^{-3}$	0.404(8)	0.566(21)	1.922(40)	0.7555(3)	[18]
DBW2 (0.87)	1.8	16	$5.69(26)\times 10^{-4}$	0.589(19)	0.780(27)	1.31(4)	0.77759(45)	[20]

TABLE V. Hadron masses computed using Wilson gauge action at $\beta=6.0$, $16^3\times 32$, $M_5=1.8$, $L_s=16$ from Ref. [28].

m_f	m_π	m_ρ	m_N
0.02	0.2687(24)	0.4530(62)	0.645(12)
0.03	0.3224(21)	0.4814(45)	0.716(5)
0.04	0.3691(19)	0.5126(42)	0.754(6)
0.05	0.4116(18)	0.5395(36)	0.805(5)

tion [19,36]. Recent quenched studies by the RBC Collaboration have shown that the chiral symmetry of DWFs is even better with a similar type of renormalization group improved gauge action, DBW2 [20]. The chiral symmetry of DWFs with DBW2 is significantly improved over the Iwasaki action. A very small additive quark mass $m_{\rm res}\sim 0.8$ MeV is achieved on a lattice with $a^{-1}\approx 1.3$ GeV and $L_s=16$. Good scaling behavior of the light hadron spectrum is observed as well [20].

To study finite volume effects numerical simulations were performed at $\beta=0.87$ ($a\approx 0.15$ fm) on two lattice sizes $8^3\times 24$ and $16^3\times 32$ with $L_s=16$ and $M_5=1.8$. Our results are analyzed on 400 quenched gauge configurations for the smaller lattice ($La\sim 1.2$ fm) and 416 configurations for the larger lattice ($La\sim 2.4$ fm). Hadron masses computed in this calculation are summarized in Table VII. Meson masses (m_π and m_ρ) for the $16^3\times 32$ lattice are evaluated from 100 configurations.

In this calculation, we utilize the sequential quark propagator method to compute three-point functions as described in Sec. II. We checked for consistency with the wall-wall method on the smaller $8^3\times 24$ lattice. The sequential- and wall-type quark propagators in the Coulomb gauge were computed at five evenly spaced values of m_f ranging from 0.02 to 0.10. The smallest quark mass corresponds to a pion mass $m_\pi\approx 390$ MeV. The nucleon source and sink were separated by about 1.5 fm, which corresponds to the same physical separation in time used in the calculation with the Wilson gauge action at $\beta=6.0$. A preliminary version of the results presented below was first reported in [34,35].

First, we check whether $Z_V=Z_A$ is true even on this coarse lattice. The vector renormalization $1/g_V^{\rm lattice}$ is plotted against the location of current insertions in Fig. 5. The data are calculated on the larger spatial volume with the sequential quark propagator method. We take a weighted average of $1/g_V^{\rm lattice}$ with the three middle points ($t-t_{\rm src}=4,5,6$) to evaluate the vector renormalization Z_V. The dependence of Z_V on m_f is shown in Fig. 6 and given in Table IX below. In

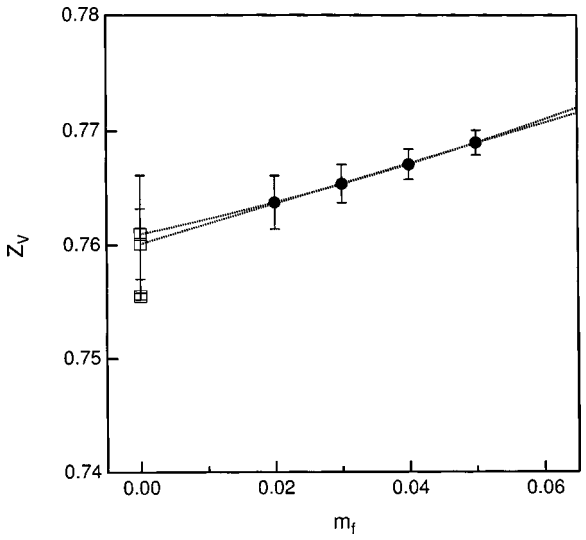

FIG. 2. Quark mass dependence of the vector current renormalization $Z_V=1/g_V^{\rm lattice}$, Wilson gauge action (note scale). Lines denote uncorrelated linear and quadratic fits to the data points. Extrapolated values are consistent with the axial-vector current renormalization computed from meson two-point functions [18,22] to less than 1%.

general $\mathcal{V}_\mu=Z_V V_\mu+O(a^2,m_f a^2)$ and $\mathcal{A}_\mu=Z_A A_\mu+O(a^2,m_f a^2)$, where $\mathcal{V}_\mu$ and $\mathcal{A}_\mu$ denote the conserved vector currents. It is not so apparent in our data. A linear extrapolation yields $Z_V=0.7952(13)$ at $m_f=0$, while a linear plus quadratic extrapolation gives the value 0.7991(25). The RBC Collaboration obtained the renormalization factor of the axial-vector current Z_A nonperturbatively from a calculation of meson two-point correlation functions [18,20]. The result found was $Z_A=0.77759(45)$ in the massless limit [20] which is smaller than the value of Z_V obtained above by 2–3 %. This discrepancy may be caused by an order $O(a^2)$ lattice artifact.

To explore this possibility further, we evaluate the renormalization factor of different vector currents. According to Sec. II, the conserved current $\mathcal{V}_\mu$ guarantees that nucleon matrix elements of $j_\mu^{\rm e.m.}$, $\mathcal{V}_\mu^d$, and $\mathcal{V}_\mu^u-\mathcal{V}_\mu^d$ should be identical. The local lattice currents V_μ^f are renormalized as $\mathcal{V}_\mu^f=Z_V^f V_\mu^f+O(a^2)=Z_V V_\mu^f+O(a^2)$ in the chiral limit. Figure 7 shows the values of Z_V^f as well as the value of Z_A from [20]. The difference among values of Z_V appears independent of m_f within statistical errors, and the discrepancy between the smallest and the largest is comparable to that between Z_V and Z_A noted above. We also note that the discrepancy is larger at

TABLE VI. Results for the nucleon axial charge, Δu, Δd, and $Z_V=1/g_V^{\rm lattice}$, Wilson gauge action, $\beta=6.0$, $16^3\times 32$, $M_5=1.8$, $L_s=16$, 400 configurations.

m_f	$(g_A)_{\rm lattice}$	$(g_A)_{\rm ren}$	$(\Delta u)_{\rm ren}$	$(\Delta d)_{\rm ren}$	Z_V
0.02	1.216(106)	0.929(82)	0.739(82)	−0.189(40)	0.7637(23)
0.03	1.380(76)	1.056(59)	0.840(54)	−0.215(26)	0.7654(17)
0.04	1.480(59)	1.135(46)	0.903(40)	−0.232(19)	0.7671(13)
0.05	1.542(47)	1.186(37)	0.942(32)	−0.243(15)	0.7689(11)

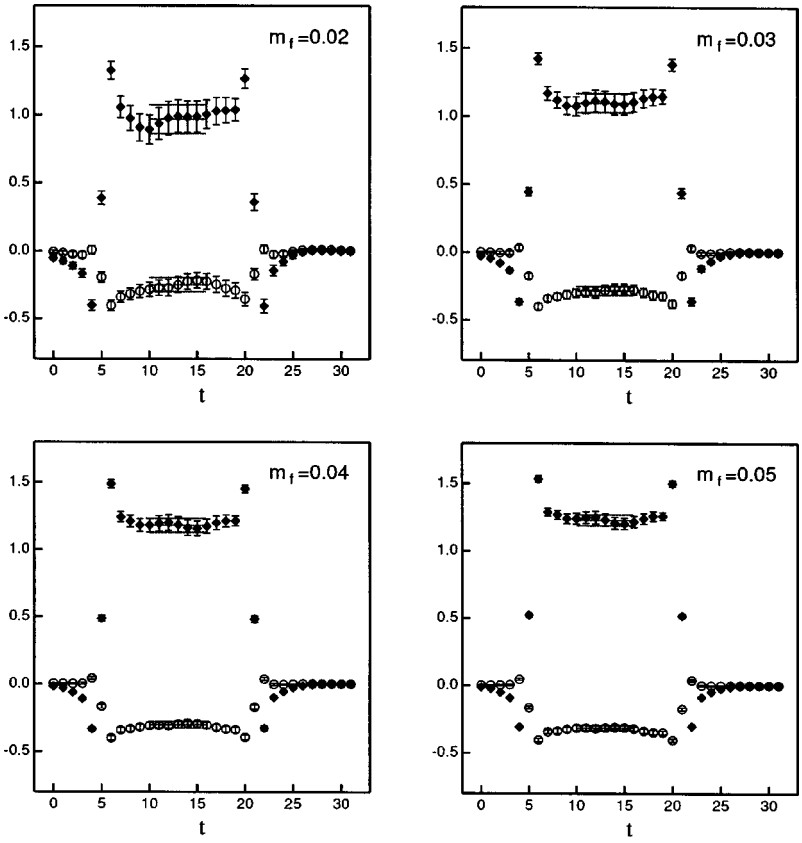

FIG. 3. The lattice estimates of the spin-dependent densities Δu (upper curves) and Δd (lower curves) for the Wilson gauge action. Decent plateaus are observed for each quark mass. The lines denote central values and statistical errors from constant fits over the plateaus.

this lattice spacing, by roughly a factor of $(1.922/1.3)^2$, than the corresponding one for the Wilson gauge action results discussed earlier. Of course, since the two gauge actions have different $O(a^2)$ errors, the comparison is only a crude one. We conclude that $Z_V = Z_A$ is satisfied up to small discretization errors of $O(a^2)$ on this coarse lattice.

In Fig. 8 we plot unrenormalized spin-dependent densities Δu and Δd, which are calculated with the sequential source propagator [30], against the location of the current insertion. In this calculation, the sequential source propagator was calculated with a box source and a point sink, so the resulting three-point function has no time reflection symmetry about the midpoint between $t_{\rm src}$ and $t_{\rm sink}$ because excited state contamination is worse for the nucleon propagating between the operator and the point sink. In Fig. 8 the plateaus appear shifted toward the wall source, as expected. Next we evaluate the bare value of $g_A^{\rm lattice} = \Delta u - \Delta d$ at each m_f, shown in Fig. 9 for both lattice volumes and tabulated in Tables VIII and IX. $g_A^{\rm lattice}$ evaluated on the smaller volume is clearly smaller for each value of m_f, and the difference increases as m_f decreases. In contrast, g_V does not show much dependence on the volume.

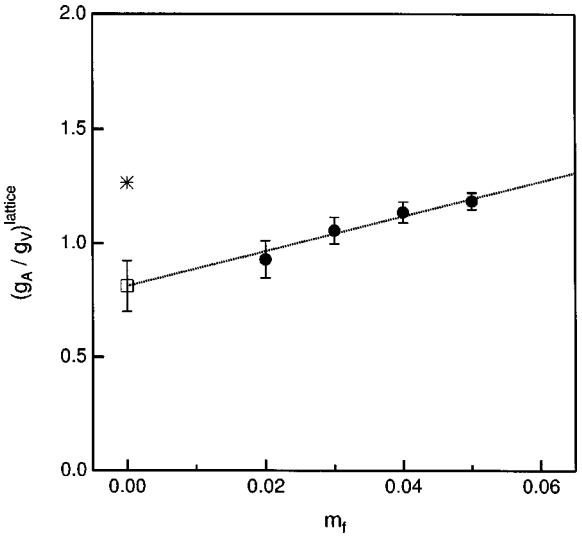

FIG. 4. The ratio of nucleon charges g_A/g_V, Wilson gauge action, $V \approx (1.6\ \text{fm})^3$. A marked decrease toward the chiral limit is evident. A linear fit significantly underestimates the experimental value (asterisk).

TABLE VII. Hadron masses computed using the DBW2 gauge action. All fits for ρ meson have $\chi^2/N_{\rm DF} < 1.0$, and < 1.5 for pion and nucleon.

$L^3 \times N_t$	m_f	m_π	m_ρ	m_N
$8^3 \times 24$	0.04	0.4255(38)	0.679(16)	1.071(13)
	0.06	0.5094(34)	0.729(9)	1.127(11)
	0.08	0.5865(30)	0.776(7)	1.205(9)
	0.10	0.6567(27)	0.823(6)	1.292(10)
$16^3 \times 32$	0.02	0.3015(16)	0.647(22)	0.854(6)
	0.04	0.4146(16)	0.681(10)	0.963(5)
	0.06	0.5050(16)	0.725(6)	1.060(4)
	0.08	0.5834(15)	0.771(5)	1.156(4)
	0.10	0.6546(14)	0.819(4)	1.242(4)

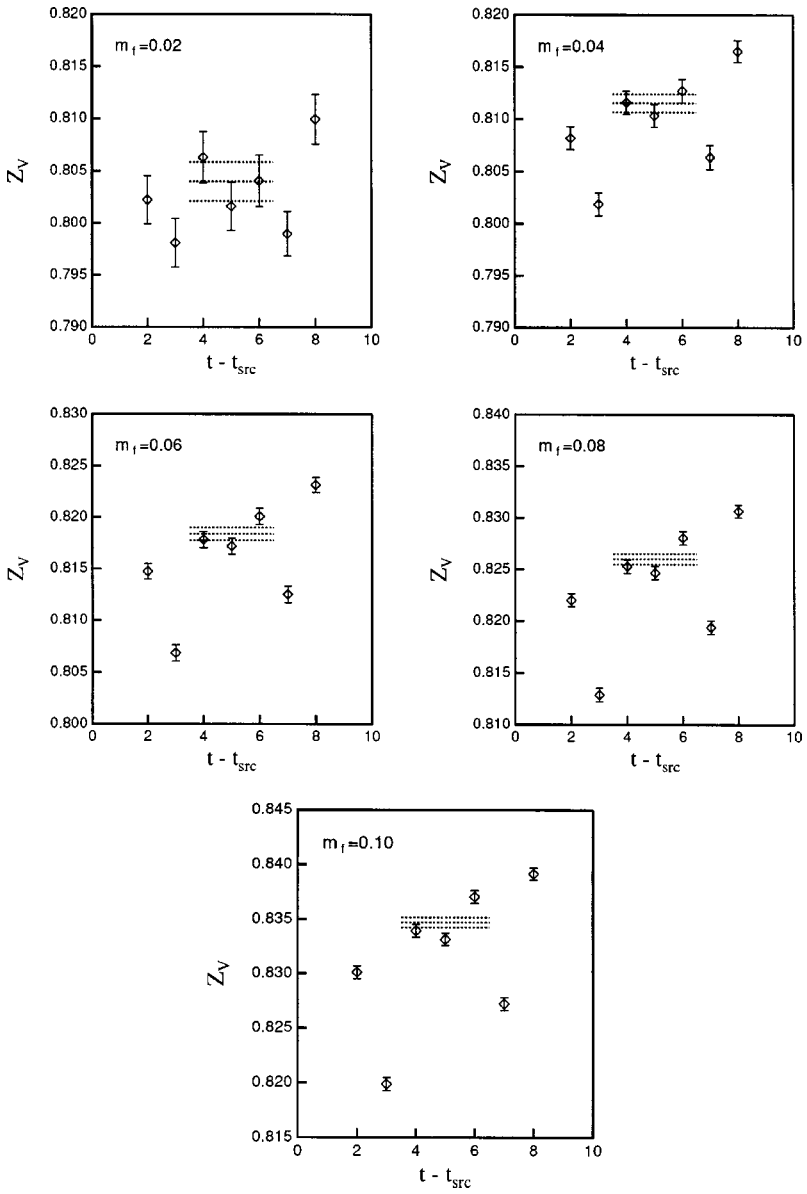

FIG. 5. $Z_V = 1/g_V^{\text{lattice}}$, DBW2 gauge action, $V \approx (2.4\ \text{fm})^3$, as a function of the current insertion time slice. Note the very fine scale, as in Fig. 1. We use the three middle points, the spread of which is less than 0.5%. The lines denote the central values and statistical errors from constant fits over them.

To compare to our previous DWF results with the Wilson gauge action, we plot the value of $(g_A/g_V)^{\text{lattice}}$ as a function of $(m_\pi/m_\rho)^2$ in Fig. 10. The smaller volume results using the DBW2 gauge action ($\beta = 0.87$) are the same (within statistical errors) as our previous results using the Wilson gauge action ($\beta = 6.0$) on a slightly larger volume. The large volume DBW2 results exhibit mild quark mass dependence while both smaller volume results show a marked decrease toward the chiral limit. We conclude that our previous DWF-Wilson-gauge-action results were significantly adversely affected by finite volume.

Finally, we extrapolate g_A^{ren} to the chiral limit. For this purpose, we have two methods. One is to extrapolate the charge ratios $(g_A/g_V)^{\text{lattice}}$ to the chiral limit where the relation $Z_V = Z_A$ is valid. The second method is the conventional one utilized in all other calculations [2–8]. The chiral extrapolation is performed on $g_A^{\text{lattice}} \times Z_A$. Recall that the latter requires the value of Z_A, whether nonperturbatively or perturbatively calculated, while the former does not. In the present case, we use the nonperturbative value of Z_A from [20].

We plot $(g_A/g_V)^{\text{lattice}}$ and $Z_A \times g_A^{\text{lattice}}$ together in Fig. 11 and perform a simple linear extrapolation in each case. The two methods provide consistent results in the chiral limit: the ratio method gives $g_A^{\text{ren}} = 1.212(27)$ while the conventional method gives $g_A^{\text{ren}} = 1.188(25)$. In light of our earlier discussion, the systematic difference, if there is one, is related to our choice of renormalization. A 2% error stemming from $Z_V \neq Z_A$ yields 0.024. This is also the difference in the central values just obtained. Thus, we quote

$$g_A^{\text{ren}} = 1.212 \pm 0.027(\text{stat}) \pm 0.024(\text{norm}), \qquad (48)$$

which underestimates the experimental value of 1.267 by less than 5%. We have not attempted to estimate residual nonzero lattice spacing, finite volume, explicit chiral symmetry breaking, and quenching effects. The first three are probably small [18–20]. The only remaining error not under good

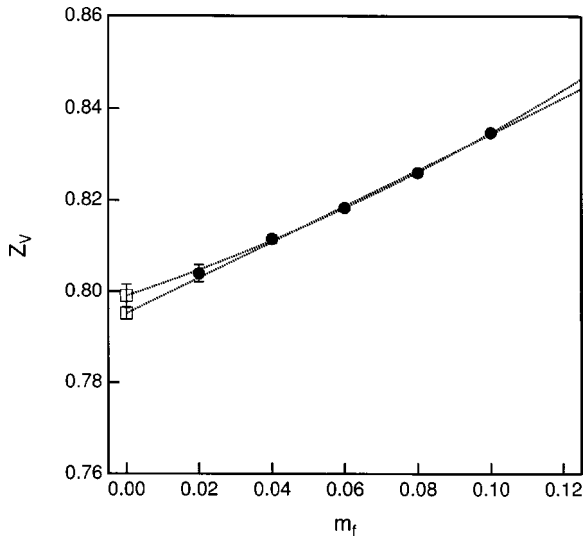

FIG. 6. Same as Fig. 2 except for the DBW2 gauge action, large volume.

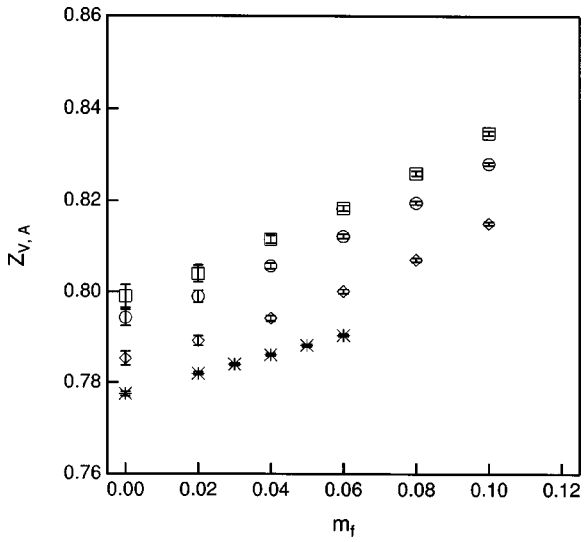

FIG. 7. Determination of the vector current renormalization from $1/g_V^{\text{lattice}}$ (squares), the electromagnetic current (circles), and the d quark current (diamonds). The axial-vector current renormalization (asterisks) [20] is shown for comparison. The different renormalization constants differ because of $O(a^2)$ lattice artifacts.

control is the quenching one which does not appear to be large [5,6], in light of the relatively good agreement with experiment shown above. This view does not change unless significant nonanalytic behavior, which we did not detect here, arises near the chiral limit.

We note that Jaffe recently showed that in the chiral limit the nucleon axial charge is delocalized, and he argued that this leads to a large reduction in g_A calculated in a finite volume surrounding the nucleon [37]. Subsequently, Cohen showed that in a finite volume with periodic boundary conditions pertaining to lattice calculations, this phenomenon does not lead to a reduction in g_A [38]. However, as emphasized in [38], this does not preclude other large finite volume effects.

As mentioned above, this calculation of g_A is performed for relatively heavy quark masses; the quenching error at this unphysically large mass scale is probably small. However, one may worry that such a calculation does not capture relevant physics in the region where the quark mass is much lighter, and the so-called ''pion cloud'' surrounding the nucleon becomes important. Nevertheless, the values of g_A^{ren} at these heavier quark masses already lie just a few percent below the experimental value and show little dependence on the quark mass. This presents an important question concerning the role of the pion cloud: is it a few percent effect, as seems plausible from our first principles calculation, or is it larger, as estimated from phenomenological models [39]?

The dependence of the product $m_N g_A$ on the lattice volume is of interest (see Fig. 12). While the smaller volume results always lie below the larger volume ones, within one standard deviation they almost always agree. There is only one exception at $am_f=0.08$ in the bare lattice result. No volume dependence is detected. This is in clear contrast to the situation of the axial charge alone. Since the product is the one that appears in the Goldberger-Treiman relation, it would be interesting to see how its counterpart, the induced pseudoscalar form factor, behaves at small momentum transfer.

IV. CONCLUSIONS

In this paper we have studied the nucleon axial charge and the vector charge in quenched lattice QCD. To capture important aspects of the chiral symmetry of QCD, we used domain wall fermions to simulate the light quarks.

We first demonstrated that the lattice renormalization of the isovector vector and axial-vector currents satisfies $Z_V = Z_A$ to a high degree of precision, less than 1% at $a^{-1} \approx 2$ GeV and about 2% at $a^{-1} \approx 1.3$ GeV. This is achieved because in practice the DWF method preserves the chiral symmetry of QCD up to small corrections and hence main-

TABLE VIII. Results for the nucleon axial charge, Δu, Δd, and $Z_V = 1/g_V^{\text{lattice}}$, DBW2 gauge action, $\beta = 0.87$, $8^3 \times 24$, $M_5 = 1.8$, $L_s = 16$, 400 configurations.

m_f	$(g_A)_{\text{lattice}}$	$(g_A)_{\text{ren}}$	$(\Delta u)_{\text{ren}}$	$(\Delta d)_{\text{ren}}$	Z_V
0.04	1.303(146)	1.059(120)	0.690(99)	−0.369(99)	0.8191(65)
0.06	1.342(74)	1.099(62)	0.817(52)	−0.282(45)	0.8242(35)
0.08	1.373(46)	1.136(39)	0.876(32)	−0.260(25)	0.8317(24)
0.10	1.398(30)	1.165(26)	0.902(21)	−0.263(15)	0.8403(18)

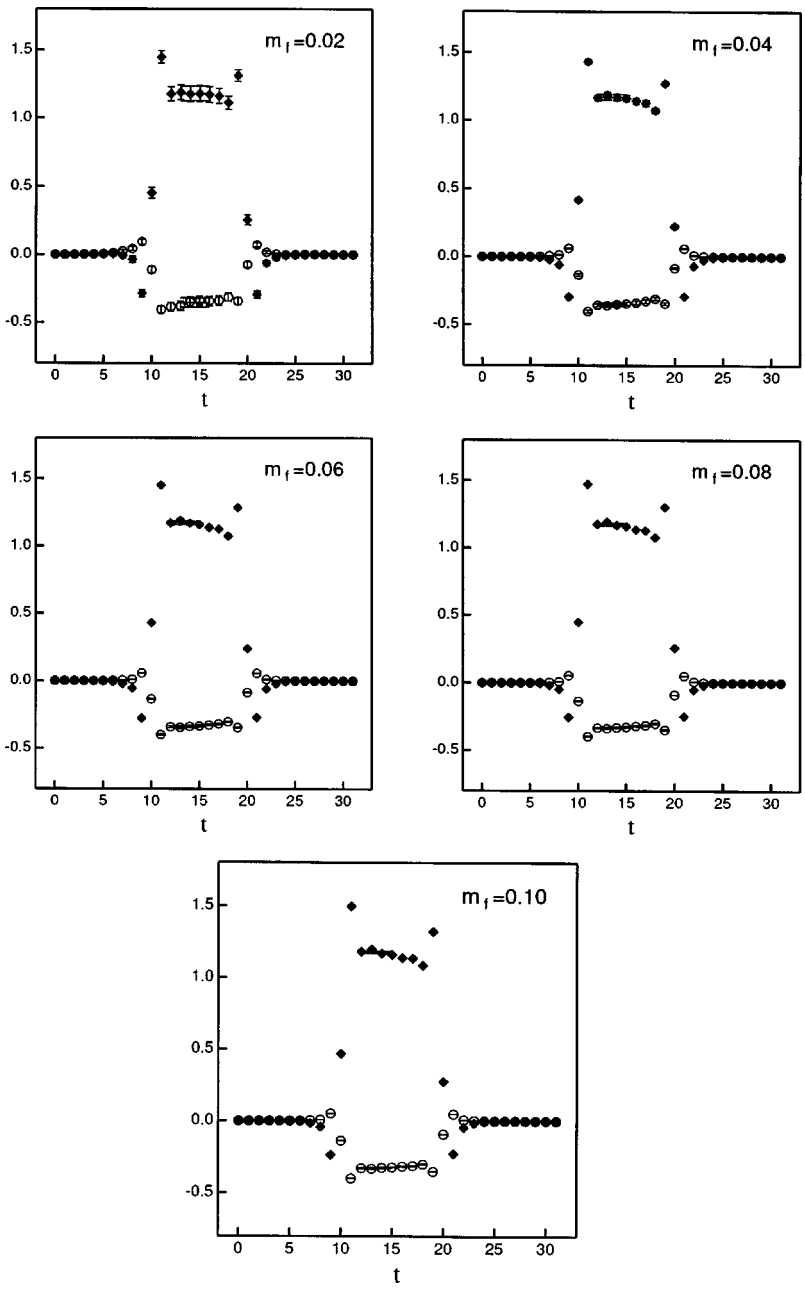

FIG. 8. Δu and Δd. Same as Fig. 3, but for the DBW2 gauge action, sequential source, and $V=(2.4\ \mathrm{fm})^3$. The plateau is shifted toward the wall source because the point sink allows more excited state contamination.

tains the relevant Ward-Takahashi identity. This holds if the underlying (quenched) gauge configuration is sufficiently smooth. Ensembles of such gauge configurations are obtained close to the continuum limit. For the single-plaquette Wilson gauge action $\beta=6.0$ ($a^{-1}\approx 2$ GeV) is good enough. For the DBW2 action the lattice spacing may be significantly larger while still maintaining good chiral symmetry ($a^{-1}\approx 1.3$ GeV).

Our first calculation of g_A with the Wilson gauge action was performed at $\beta=6.0$ on a $16^3\times 32$ lattice. The corre-

TABLE IX. Results for the nucleon axial charge, Δu, Δd, and $Z_V=1/g_V^{\mathrm{lattice}}$, DBW2 gauge action, $\beta=0.87$, $16^3\times 32$, $M_5=1.8$, $L_s=16$, 416 configurations.

m_f	$(g_A)_{\mathrm{lattice}}$	$(g_A)_{\mathrm{ren}}$	$(\Delta u)_{\mathrm{ren}}$	$(\Delta d)_{\mathrm{ren}}$	Z_V
0.02	1.531(60)	1.229(49)	0.945(44)	−0.284(27)	0.8040(19)
0.04	1.523(24)	1.230(20)	0.946(17)	−0.284(10)	0.8115(9)
0.06	1.510(15)	1.230(12)	0.953(10)	−0.277(6)	0.8184(6)
0.08	1.505(11)	1.236(9)	0.963(7)	−0.273(4)	0.8260(5)
0.10	1.503(8)	1.246(7)	0.975(6)	−0.271(3)	0.8347(5)

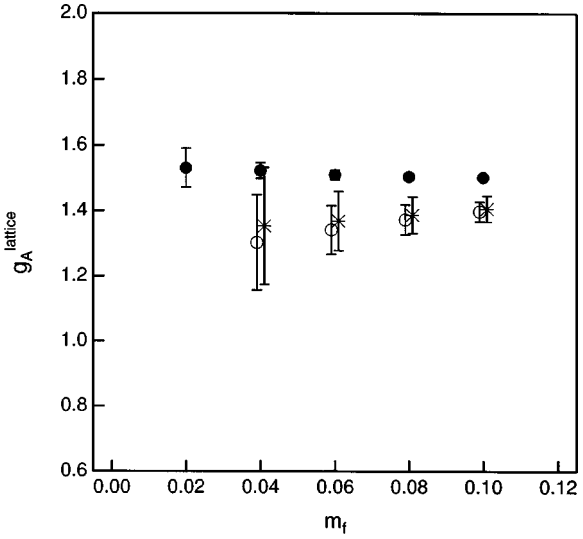

FIG. 9. Dependence of the unrenormalized nucleon axial charge on quark mass and lattice volume. Results from the sequential source method (circles) and the wall source method (asterisks) on the smaller lattice show good agreement. The sequential method provides somewhat smaller statistical errors than the wall method. The larger lattice results (solid circles), obtained with the sequential method, exhibit higher values than the smaller lattice ones over the entire range of quark mass studied.

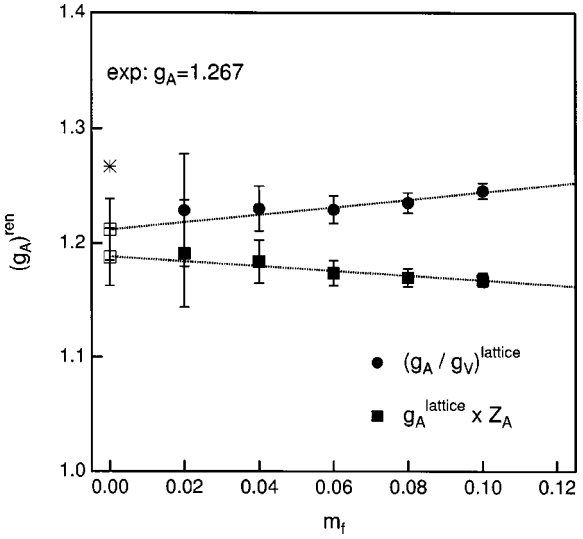

FIG. 11. Two methods to obtain the physical nucleon axial charge, the ratio of axial-vector to vector charge (circles), and the lattice axial-vector charge times the axial-vector current renormalization factor Z_A in the chiral limit from Ref. [20]. They show slightly different quark mass dependence, but extrapolate to consistent values. Each underestimates the experimental value (asterisk) by roughly 5%.

sponding spatial volume $\sim(1.6\ \mathrm{fm})^3$ is similar to those used in previous lattice calculations. This volume is rather small in comparison with the experimentally measured proton charge radius. On this lattice we found that all the relevant three-point functions are well behaved and that we can reliably extract the charges. The isovector vector current renormalization Z_V determined from them agrees well with the corresponding axial current renormalization Z_A, independently obtained from the axial Ward-Takahashi identity. We found that both the axial charge g_A^{lattice} and its ratio to the vector charge $(g_A/g_V)^{\mathrm{lattice}}$ exhibit a very strong dependence on the quark mass. A simple linear extrapolation of $(g_A/g_V)^{\mathrm{lattice}}$ to zero quark mass yielded a very small value, about 2/3 of the experimental one.

The second quenched calculation employed the DBW2 gauge action with $\beta=0.87$ set for a coarser lattice spacing, $a\approx 0.15$ fm. This allowed a larger physical volume while maintaining good chiral symmetry. To study pure finite vol-

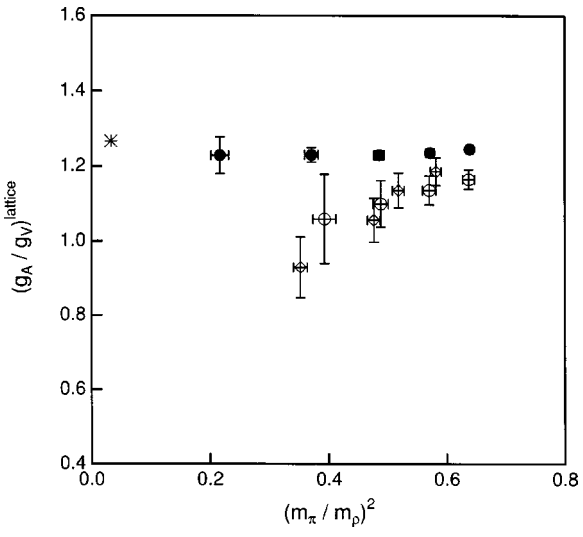

FIG. 10. The physical ratio of nucleon charges. DBW2 gauge action results on two different physical volumes $(2.4\ \mathrm{fm})^3$ (solid circles) and $(1.2\ \mathrm{fm})^3$ (open circles) reveal the existence of a significant finite volume effect. Wilson gauge action results (diamonds), $V\approx(1.6\ \mathrm{fm})^3$, also appear to be affected by finite volume.

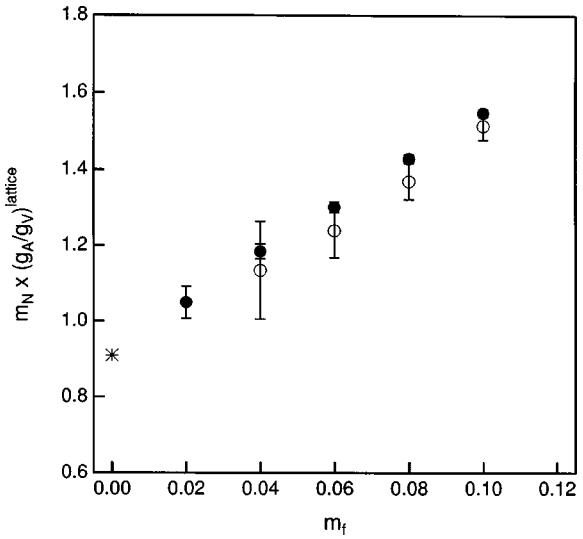

FIG. 12. The lattice volume and quark mass dependences of the product $m_N g_A$ (renormalized). Closed (large volume) and open (small volume) circles. All agree within one standard deviation. No volume dependence is detected.

ume effects, at fixed lattice spacing we calculated on lattices with sizes $16^3\times 32$ and $8^3\times 24$ [$\sim$(1.2 fm)^3 and $\sim$(2.4 fm)^3, respectively]. A significant dependence on the volume is seen in both the axial charge $g_A^{\rm lattice}$ and the charge ratio $(g_A/g_V)^{\rm lattice}$, with the larger volume giving larger values. In contrast, g_V does not show such dependence. The dependence on the quark mass is also different. In the larger volume the central values remain almost constant, while in the smaller volume they decrease noticeably with the quark mass. In the chiral limit the two differ by about 20%. The behavior of g_A in the smaller volume is quite consistent with that observed in the earlier calculation with the Wilson gauge action.

Our estimate of $(g_A/g_V)^{\rm ren}$ at zero quark mass from the larger volume with DBW2 action is $1.212\pm 0.027({\rm stat})\pm 0.024({\rm norm})$. The systematic error is estimated from the 2% difference between Z_A and Z_V which are theoretically equivalent to $O(a^2)$, neglecting even smaller effects induced by explicit chiral symmetry breaking in DWFs. It underestimates the experimental value of 1.2670(30) by less than 5%. This discrepancy is smaller than twice the theoretical error.

Thus dependence on the volume seems to be the largest among the known sources of systematic error for the first principles lattice calculation of g_A. This suggests that close attention be paid to the finite volume effect in other lattice numerical studies of nucleon structure, in particular the moments of spin-polarized structure functions, which are related to the axial charge.

It should also be noted that although the crucial relation $Z_V=Z_A$ is satisfied well in the second calculation, we detected small $O(a^2)$ differences among different determinations of Z_V. Such differences were not detectable in the first set of simulations with the Wilson gauge action at $a\approx 0.10$ fm. Numerically this is at most a few percent effect and does not affect the volume dependence.

As discussed at the end of Sec. III, the present calculation of g_A was performed using relatively heavy quark masses ($390\leqslant m_\pi\leqslant 860$ MeV) so that the systematic error arising from quenching may be small. However, one may worry that such a calculation does not capture the physics of the pion cloud surrounding the nucleon. In spite of this, the values of $g_A^{\rm ren}$ at these unphysically heavy quark masses lie just below the experimental value and show little, if any, dependence on the quark mass. It is also interesting to note that the product $m_N g_A$ shows noticeably less volume dependence. Since this is the combination that appears in the Goldberger-Treiman relation, it would be interesting to see how its counterpart, the induced pseudoscalar form factor, behaves at small but nonzero nucleon momentum.

ACKNOWLEDGMENTS

We thank Roger Horsley for his private communication providing the clover results prior to publication. We also thank the other members, current and past, of the RIKEN-BNL-Columbia (RBC) Collaboration. In particular, we thank Yasumichi Aoki for his help in optimizing the box source size, Norman Christ for his careful reading of the manuscript, and Chris Dawson for helpful discussion on $O(a^2,m_f a^2)$ corrections in local current renormalization. Thanks are also due to RIKEN, Brookhaven National Laboratory, and the U.S. Department of Energy for providing the facilities essential for the completion of this work. The numerical calculations were done on the 600 Gflops QCDSP computer at the RIKEN-BNL Research Center. S.S. thanks the JSPS for a Grant-in-Aid for Encouragement of Young Scientists (No. 13740146).

APPENDIX: CURRENT ALGEBRA AND CVC HYPOTHESIS

Defining the charge $\mathcal{Q}_V^a=i\int d^3x\, V_0^a(\vec{x},t)$,[2] the transformation for the quark fields in the isospin SU(2) subgroup of the SU(2)$\times$SU(2) chiral symmetry can be represented by

$$[\mathcal{Q}_V^a,\psi(x)]=-T^a\psi(x), \tag{A1}$$

$$[\mathcal{Q}_V^a,\bar{\psi}(x)]=+\bar{\psi}(x)T^a, \tag{A2}$$

where $\psi=(u,d)^T$ and $V_\mu^a(x)=\bar{\psi}(x)\gamma_\mu T^a\psi(x)$. One can easily find that the axial current $A_\mu^a(x)=\bar{\psi}(x)\gamma_5\gamma_\mu T^a\psi(x)$ and vector current V_μ^a transform under isospin symmetry as

$$[\mathcal{Q}_V^a,V_\mu^b(x)]=i\varepsilon_{abc}V_\mu^c(x), \tag{A3}$$

$$[\mathcal{Q}_V^a,A_\mu^b(x)]=i\varepsilon_{abc}A_\mu^c(x). \tag{A4}$$

According to the above SU(2) current algebra, A_μ^+ and V_μ^+ can be expressed as

$$A_\mu^\pm(x)=\bar{\psi}(x)\gamma_\mu\gamma_5 T^\pm\psi(x)=-[\mathcal{Q}_V^\pm,A_\mu^3(x)], \tag{A5}$$

$$V_\mu^\pm(x)=\bar{\psi}(x)\gamma_\mu T^\pm\psi(x)=-[\mathcal{Q}_V^\pm,V_\mu^3(x)], \tag{A6}$$

where $T^\pm=T_1\pm iT_2$. Hence, under the CVC hypothesis, one can find

$$\begin{aligned}\langle p|A_\mu^+|n\rangle&=-\langle p|[\mathcal{Q}_V^+,A_\mu^3]|n\rangle\\&=-\langle p|\mathcal{Q}_V^+A_\mu^3|n\rangle+\langle p|A_\mu^3\mathcal{Q}_V^+|n\rangle\\&=\langle p|A_\mu^3|p\rangle-\langle n|A_\mu^3|n\rangle=2\langle p|A_\mu^3|p\rangle.\end{aligned} \tag{A7}$$

The third line follows from $\mathcal{Q}_V^+|n\rangle=|p\rangle$ and $\langle p|\mathcal{Q}_V^+=\langle n|$. A similar calculation for the vector case yields the relation $\langle p|V_\mu^+|n\rangle=2\langle p|V_\mu^3|p\rangle$.

[2]This definition of $\mathcal{Q}_V^a$ is slightly different from the one in [28]. The only difference is a factor of $i/2$.

[1] Particle Data Group, K. Hagiwara *et al.*, Phys. Rev. D **66**, 010001 (2002).
[2] M. Fukugita, Y. Kuramashi, M. Okawa, and A. Ukawa, Phys. Rev. Lett. **75**, 2092 (1995).
[3] K. F. Liu, S. J. Dong, T. Draper, J. M. Wu, and W. Wilcox, Phys. Rev. D **49**, 4755 (1994).
[4] M. Göckeler, R. Horsley, E. M. Ilgenfritz, H. Perlt, P. Rakow, G. Schierholz, and A. Schiller, Phys. Rev. D **53**, 2317 (1996).
[5] TXL Collaboration, S. Güsken *et al.*, Phys. Rev. D **59**, 114502 (1999).
[6] LHPC and SESAM Collaborations, D. Dolgov *et al.*, Phys. Rev. D **66**, 034506 (2002).
[7] S. Capitani *et al.*, Nucl. Phys. B (Proc. Suppl.) **79**, 548 (1999).
[8] UKQCD Collaboration, R. Horsley, Nucl. Phys. B (Proc. Suppl.) **94**, 307 (2001).
[9] M. L. Goldberger and S. B. Treiman, Phys. Rev. **110**, 1178 (1958).
[10] M. Gell-Mann, R. J. Oakes, and B. Renner, Phys. Rev. **175**, 2195 (1968).
[11] D. B. Kaplan, Phys. Lett. B **288**, 342 (1992).
[12] Y. Shamir, Nucl. Phys. **B406**, 90 (1993).
[13] R. Narayanan and H. Neuberger, Phys. Lett. B **302**, 62 (1993).
[14] V. Furman and Y. Shamir, Nucl. Phys. **B439**, 54 (1995).
[15] Y. Kikukawa, Nucl. Phys. **B584**, 511 (2000).
[16] P. Hernandez, K. Jansen, and M. Luscher, Nucl. Phys. **B552**, 363 (1999).
[17] P. Hernandez, K. Jansen, and M. Luscher, hep-lat/0007015.
[18] RBC Collaboration, T. Blum *et al.*, hep-lat/0007038.
[19] CP-PACS Collaboration, A. Ali Khan *et al.*, Phys. Rev. D **63**, 114504 (2001).
[20] RBC Collaboration, Y. Aoki *et al.*, hep-lat/0211023.
[21] T. Blum, Nucl. Phys. B (Proc. Suppl.) **73**, 167 (1999).
[22] T. Blum *et al.*, Phys. Rev. D **66**, 014504 (2002).
[23] T. Blum and S. Sasaki, hep-lat/0002019.
[24] T. Blum, S. Ohta, and S. Sasaki, Nucl. Phys. B (Proc. Suppl.) **94**, 295 (2001).
[25] N. Isgur and G. Karl, Phys. Rev. D **20**, 1191 (1979).
[26] A. Chodos, R. L. Jaffe, K. Johnson, and C. B. Thorn, Phys. Rev. D **10**, 2599 (1974).
[27] T. Takaishi, Phys. Rev. D **54**, 1050 (1996).
[28] S. Sasaki, T. Blum, and S. Ohta, Phys. Rev. D **65**, 074503 (2002).
[29] R. M. Woloshyn and K. F. Liu, Nucl. Phys. **B311**, 527 (1989).
[30] G. Martinelli and C. T. Sachrajda, Nucl. Phys. **B316**, 355 (1989).
[31] C. W. Bernard, T. Draper, G. Hockney, and A. Soni, in Proceedings, Wuppertal 1985 Lattice Gauge Theory, 1985, p. 199.
[32] M. Kim and S. Kim, Phys. Rev. D **58**, 074509 (1998).
[33] E. Jenkins and A. V. Manohar, Phys. Lett. B **259**, 353 (1991).
[34] RBC Collaboration, S. Sasaki, T. Blum, S. Ohta, and K. Orginos, Nucl. Phys. B (Proc. Suppl.) **106**, 302 (2002).
[35] RBC Collaboration, S. Ohta, hep-lat/0210006.
[36] RIKEN-BNL-CU Collaboration, L. L. Wu, Nucl. Phys. B (Proc. Suppl.) **83**, 224 (2000).
[37] R. L. Jaffe, Phys. Lett. B **529**, 105 (2002).
[38] T. D. Cohen, Phys. Lett. B **529**, 50 (2002).
[39] W. Detmold, W. Melnitchouk, and A. W. Thomas, Phys. Rev. D **66**, 054501 (2002).